M&C 2017 - International Conference on Mathematics & Computational Methods Applied to Nuclear Science & Engineering, Jeju, Korea, April 16-20, 2017, on USB (2017)

Development of the high-fidelity neutronics and thermal-hydraulic coupling code NECP-X/SUBSC

Jun Chen, Liangzhi Cao, Zhouyu Liu*, Hongchun Wu, Chen Zhao, Qingming He

School of Nuclear Science and Technology, Xi'an Jiaotong University, Xi'an Shaanxi 710049, China
scutcjun@163.com; caolz@mail.xjtu.edu.cn; zhouyuliu@mail.xjtu.edu.cn; hongchun@mail.xjtu.edu.cn; okzhaochen@163.com; he_qing_ming@foxmail.com

Abstract *The development and verification of a coupling code named NECP-X/SUBSC which integrates a high-fidelity neutronics code NECP-X and a thermal-hydraulics subchannel code SUBSC are presented. In order to accomplish high-fidelity, improved and realistic geometry modeling such as semi-explicit representation of grid spacer, 2D/1D fusion method and resonance self-shielding treatment with pesudo-resonant-nuclide subgroup method are investigated. A group of benchmark problems including VERA core physics benchmark progression problems 1-3 are utilized to verify NECP-X. Then an internal coupling method is adopted to integrate SUSBC with NECP-X. The coupling code NECP-X/SUBSC is first applied to a simplified PWR 3×3 pin cluster case. Afterwards, VERA core physics benchmark problem #6, 3D Hot Full Power (HFP) is simulated. eigenvalue and normalized radial power distribution are compared to results from CASL's MPACT/CTF coupling code.*

Key Words: high-fidelity, NECP-X, SUBSC, coupling

I. INTRODUCTION

Recently, several solutions, including power updates, lifetime extension and higher burnup, have been proposed to improve the economic competitiveness of nuclear energy[1]. These solutions will aggravate some industry challenge problems, such as CRUD-induced power shift, CRUD-induced localized corrosion, pellet clad interation[2-3] etc. Essentially, these problems are multi-physics coupling phenomenon, which needs neutron transport, thermal-hydraulics, fuel performance and corrosion chemistry coupling calculation to perform accurate modeling and simulation. Among these multiple physics phenomena, the neutronics and thermal-hydraulics (T/H) are the basic ones [4]. With the steady growth of computation capability, the coupling of high-fidelity neutronics and thermal-hydraulics becomes more and more popular worldwide. Various high-fidelity coupling codes have been released including nTRACER/MATRA[4], MPACT/CTF[5], MC21/COBRA-IE[6], Serpent 2/SUBCHANFLOW[7], etc. Both deterministic and Monte Carlo methods are employed to solve the neutron transport problem, while sub-channel code is utilized as the T/H solver by most research groups working on the high-fidelity reactor simulation. The main reasons are that the computational fluid dynamics approach is not yet mature enough in the nuclear engineering field and its computational burden is unacceptable[7].

In this paper, an internal coupling of a newly developed high-fidelity neutronics code NECP-X and an in-house sub-channel code SUBSC is presented. The paper is organized as follows. In section Ⅱ, the neutronics models of NECP-X are described. In section Ⅲ, basic equations and numerical approaches of SUBSC are given. The verification results of NECP-X are shown in section Ⅳ. Coupling NECP-X with SUBSC as well as its initial application are presented in section Ⅴ. Conclusions are summarized in section Ⅵ.

II. NEUTRONICS MODELS OF NECP-X

1. 2D/1D fusion method

The detailed 2D/1D fusion method[8] and its verification have been presented in the companionate paper[9].

2. Resonance self-shielding treatment with the pseudo-resonant-nuclide subgroup method

The challenges of resonance treatments encountered in the neutronics and thermal-hydraulic coupling calculation are large scale, resonance interference effect and temperature distribution effect. To settle these challenges, the pseudo-resonant-nuclide subgroup method is proposed.

Firstly, the whole problem is split to multiple equivalent 1-D cylindrical problems by preserving Dancoff correction factor of each pin cell. The Dancoff correction factors are calculated by neutron current method, which adopts MOC as the fixed source transport solver. The Dancoff correction factor is defined as

$$C = \frac{\phi_0 - \phi}{\phi_0}$$

where ϕ_0 is the flux of the target fuel pin in the isolated system; ϕ is the flux of the target fuel pin in the lattice system. The outer radius of the equivalent 1-D problem is obtained by binary search, the aim of which is to preserve the Dancoff correction factor calculated in the previous step.

Secondly the equivalent 1-D problems are solved independently by pseudo-resonant-nuclide subgroup method. The pseudo nuclide is nuclide that mixed by all the resonant nuclides of the equivalent 1-D problem according to their number density ratios. The cross section table (total cross sections, scattering cross sections, absorption cross sections and neutron production cross sections against dilution cross sections of the pseudo resonant nuclide and the component resonant nuclides) is obtained by solving hyper-fine energy group (~1M energy groups) 0-D neutron slowing-down problems. As all the resonant nuclides are mixed in the slowing-down problems, the resonance interference effect is considered in the cross section table. Then the physical probability table for the pseudo resonant nuclide and the component resonant nuclides are obtained by fitting the cross section table.

The subgroup fixed source equation[10-11] formulated based on pseudo resonant nuclide is solved by collision probability method:

$$V_n \Sigma_{t,n,i} \phi_{n,i} = \sum_{m=1}^{N} V_m P_{m \to n,i} Q_{n,i}$$

Where V_n is the volume of region n, $\Sigma_{t,n,i}$ is macroscopic subgroup cross section, $\phi_{n,i}$ is subgroup flux, $P_{m \to n,i}$ is the collision probability, $Q_{n,i}$ is the scattering source.

Finally the effective self-shielding cross sections are obtained as:

$$\sigma_{x,k,n,g}^{\text{eff}} = \mu_{n,g} \frac{\int_{\Delta u_g} \sigma_{x,k}(u) \phi_n(u) \mathrm{d}u}{\int_{\Delta u_g} \phi_n(u) \mathrm{d}u} = \mu_{n,g} \frac{\sum_{i=1}^{I} \sigma_{x,k,g,i} \phi_{n,g,i}}{\sum_{i=1}^{I} \phi_{n,g,i}}$$

Where $\mu_{n,g}$ is the SPH correction factor.

The temperature distribution effect of the moderator only affects the number density of the moderator in the resonance energy range. Therefore this effect is considered in the Dancoff calculation by changing the number densities. The temperature distribution effect affects both the number density and the microscopic cross sections of the resonant nuclides in the fuel. The change of number density can be easily considered in the subgroup method. As the equivalent 1-D problems are independent, only one temperature is assumed for the resonant nuclides in the equivalent 1-D problem when the effective temperature is used. This problem can be easily solved by the pseudo-resonant-nuclide subgroup method described above. Therefore different fuel temperatures of different pin cells can be considered.

III. SUB-CHANNEL CODE SUBSC

In the high-fidelity coupling calculation, the accurate T/H feedback is essential to provide the temperature and atom number density distributions of fuel, cladding and coolant. Compared to the simple closed channel T/H model and the CFD method, the sub-channel approach has a better balance between accuracy and efficiency especially when dealing with the whole core thermal-hydraulics calculation. The in-house sub-channel code SUBSC is employed as the T/H solver whose basic theory is given in the following part.

1. Conservation equations and numerical approach

For an axial control volume unit "j" in channel "i" surrounded by volumes of neighboring channel "n" through a gap k (see Fig. 1 and Fig. 2), SUBSC employs homogeneous equilibrium method for the two-phase calculation, assuming that the homogenous mixture of fluid and vapor is at thermal equilibrium.

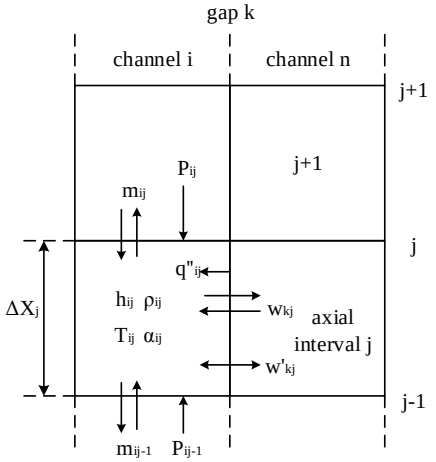

Fig. 1. Control volume for mass, energy, and axial momentum balance equations (lateral view).

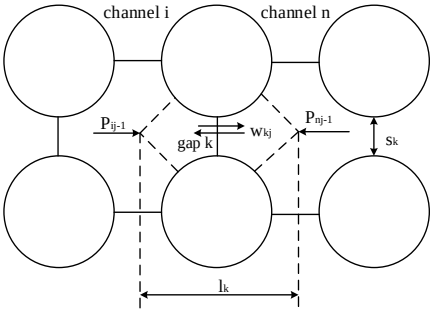

Fig. 2. Control volume for lateral momentum balance finite-difference equation (top view)

The mass conservation equation:

$$A_i \frac{\Delta X_j}{\Delta t} \left(\rho_{ij} - \rho_{ij}^n \right) + m_{ij} - m_{ij-1} + \Delta X_j \sum_{k \in i} e_{ik} w_{kj} = 0 \quad (1)$$

The energy conservation equation:

$$\frac{A_i}{\Delta t} \left[\rho''_{ij} \left(h_{ij} - h_{ij}^n \right) + h_{ij} \left(\rho_{ij} - \rho_{ij}^n \right) \right] + \frac{1}{\Delta X_j} \left(m_{ij} h_{ij}^* - m_{ij-1} h_{ij-1}^* \right) + \sum_{k \in i} e_{ik} w_{kj} h_{kj}^* = \sum_{r \in i} P_{ir} q''_{rj} - \sum_{k \in i} w'_{kj} \left(h_{ij} - h_{nj} \right) - \sum_{k \in i} C_k s_k \left(T_{ij} - T_{nj} \right) \quad (2)$$

The axial momentum equation:

$$\frac{\Delta X_j}{\Delta t}\left(m_{ij}-m_{ij}^n\right)+m_{ij}U'_{ij}-m_{ij-1}U'_{ij\text{-}1}+\Delta X_j\sum_{k\in i}e_{ik}w_{kj}U'^{*}_{kj}=$$
$$-A_l\left(P_{ij}-P_{ij\text{-}1}\right)-gA_l\Delta X_j\rho_{ij}\cos\theta-f_T\Delta X_j\sum_{k\in i}w'_{kj}\left(U'_{ij}-U'_{nj}\right) \quad (3)$$
$$-\frac{1}{2}\left(\frac{\Delta X_j f_{ij}\varphi^2}{D_h\rho_{ij}}+K_{ij}v'^{*}+\left(\frac{1}{\rho_{ij}}-\frac{1}{\rho_{ij-1}}\right)\right)|m_{ij}|\frac{m_{ij}}{A_l}$$

The lateral momentum equation:

$$\frac{\Delta X_j}{\Delta t}\left(w_{kj}-w_{kj}^n\right)+\overline{U'}_{kj}w^*_{kj}-\overline{U'}_{kj-1}w^*_{kj\text{-}1}=\frac{s_k}{l_k}\Delta X_j P_{kj-1}-\frac{1}{2}\left(K_G\frac{\Delta X v'^{*}}{s_k l_k}\right)_{kj}|w_{kj}|w_{kj} \quad (4)$$

The heat flux in the energy equation is calculated from heat transfer in the fuel rod by solving the following 3-D (radial-axial-azimuthal) conduction equation.

$$\rho c_p\frac{\partial T}{\partial t}=\frac{1}{r}\frac{\partial}{\partial r}\left(\lambda\cdot r\frac{\partial T}{\partial r}\right)+\frac{1}{r^2}\frac{\partial}{\partial\varphi}\left(\lambda\frac{\partial T}{\partial\varphi}\right)+\frac{\partial}{\partial z}\left(\lambda\frac{\partial T}{\partial z}\right)+S \quad (5)$$

2. Numerical methodology

The four coupled equations (1)-(4) form a nonlinear system and can be solved iteratively with Newton-Raphson method. In each iteration, an axial sweep is performed from the inlet to the outlet. For each axial layer, the mixture enthalpies are calculated first from the energy conservation equation; the volume temperatures and the mixture density can be updated. Then axial and lateral flow rates can be solved with a tentative pressure. Finally the pressure correction equation (mass equation) is solved to get the pressure correction δP and update the tentative pressure and flow rates as follows:

$$P_{ij}=\hat{P}_{ij}+\delta P_{ij}$$
$$m_{ij}=\hat{m}_{ij}+\frac{\partial m_{ij}}{\partial P_{ij}}\left(\delta P_{ij}-\delta P_{ij-1}\right) \quad (6)$$
$$w_{kj}=\hat{w}_{kj}+\frac{\partial w_{kj}}{\partial P_{kj-1}}\left(\delta P_{lj-1}-\delta P_{l'j-1}\right)$$

where the hat mark means the value of previous iteration.

Ⅳ. ASSESSMENT OF NECP-X SOLUTIONS

In order to assess the effectiveness of 2D/1D fusion method and the resonance self-shielding models, NECP-X was applied to the VERA benchmark problems 1-3[9]. The in-house 69-group cross section library NECL generated from the ENDF-B/VII.0 is used. The inflow transport approximation is adopted to generate accurate transport cross sections. The ray spacing used is 0.03cm except for the integral fuel burnable absorber (IFBA) for which the ray spacing is set to be 0.01 cm. 16 azimuthal and 3 polar angles per octant are employed.

1. VERA 2D benchmark analysis

The reference solutions of VERA 2D benchmark were obtained by SCALE Monte Carlo code KENO-VI[12]. Comparisons of eigenvalue and normalized pin power distributions between KENO-VI and NECP-X for the VERA progression problem 1 (2D pin cell) and 2 (2D lattice) are given in table 1. It shows that the NECP-X results for eigenvalue and pin power distributions agree well with the reference. Maximum error of eigenvalue is -325 pcm for 2H lattice case containing 24 boron carbide (B_4C) control rods. Maximum pin power error and root mean square (RMS) pin power error are 0.20%and 0.59% respectively.

Table 1. Comparison of eigenvalue and pin powers for VERA progression problems 1 and 2

Case	KENO-VI (SD in pcm)	NECP-X	Δk(pcm)	Pin RMS error(%)	Pin Max error(%)
1A	1.18704(5)	1.18712	8	-	-
1B	1.18215(7)	1.18218	3	-	-
1C	1.17172(7)	1.17151	-21	-	-
1D	1.16260(7)	1.16248	-12	-	-
1E	0.77170(8)	0.77071	-99	-	-
2A	1.18218(2)	1.18229	11	0.07	-0.14
2B	1.18336(2)	1.18346	10	0.07	-0.16
2C	1.17375(2)	1.17380	5	0.08	-0.14
2D	1.16559(2)	1.16553	-6	0.07	-0.15
2E	1.06963(2)	1.07015	52	0.07	-0.15
2F	0.97602(3)	0.97674	72	0.11	0.24
2G	0.84770(3)	0.84662	-108	0.18	0.35
2H	0.78822(3)	0.79147	325	0.20	0.59
2I	1.17992(2)	1.18006	14	0.07	-0.18
2J	0.97519(3)	0.97600	81	0.10	0.22
2K	1.02006(3)	1.02098	92	0.11	0.26
2L	1.01892(2)	1.01786	-106	0.11	-0.22
2M	0.93880(3)	0.93727	-153	0.11	-0.22
2N	0.86962(3)	0.86846	-116	0.12	-0.24
2Q	1.17194(2)	1.17093	-101	0.08	0.17

2. VERA 3D HZP assembly problem

The assembly geometry is modeled as explicitly as possible. Detailed axial reflector regions, including plenum, end plugs, end gaps are simulated explicitly. The grid spacer semi-explicit representation is done as in problem 2Q by dividing the grid mass equally amongst the 289 lattice cells and placing that mass in an equivalent volume box on the outside of each cell.

Due to large negative self-scattering cross-section caused by the inflow transport correction, the convergence of 2D/1D iteration calculation is degraded. Therefore, P0 approximation for the scattering source was adopted to calculate the 3D HFP assembly of problem 3A.

Comparison of eigenvalue is provided in Table 2. Compared to KENO-VI, NECP-X underestimates eigenvalue by 31 pcm.

Table 2. Comparison of eigenvalue for VERA progression problems 3A

Code	Eigenvalue
KENO-VI	1.17572±0.000005
NECP-X	1.17603

Fig. 3 shows relative error of normalized radial power distribution between NECP-X and KENO-VI results. Maximum error and RMS error are 0.74% and 0.43% respectively. Fig. 4 provides the axial comparison, which shows good agreement and demonstrates the capability of accounting for spacer grids on cross section processing.

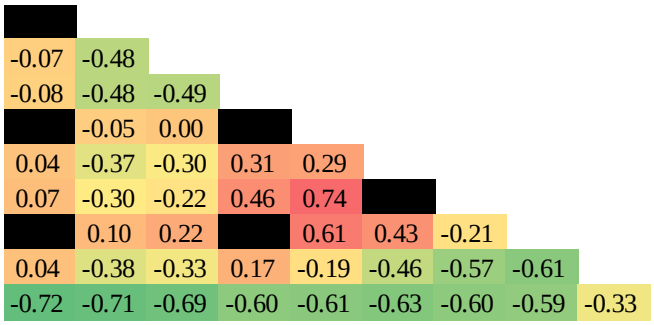

Fig. 3. Relative error of radial power distribution between NECP-X and KENO-VI

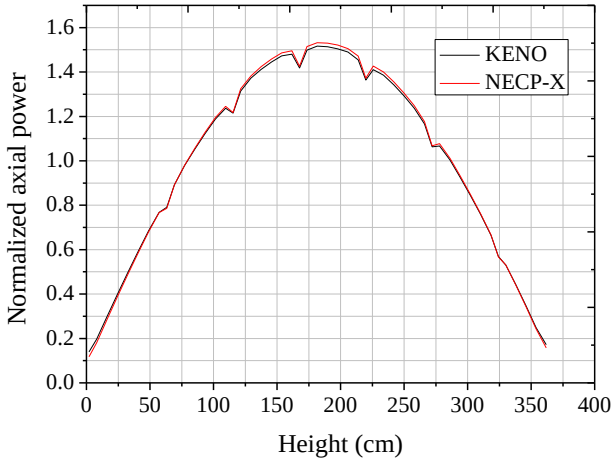

Fig. 4. Comparison of normalized axial power distribution between NECP-X and KENO-VI for problem 3A

Ⅴ. COUPLING NECP-X WITH SUBSC

The nonlinear relationship between different physical quantities associated with neutronics and thermal-hydraulics has been a challenging problem in coupling these two codes. Several numerical solution strategies have been investigated, such as Newton method, fixed point iteration, JFNK, etc[12].

Fixed point iteration, which is the simplest and perhaps most common approach is used in this paper. This strategy is performed by sequentially solving NECP-X and SUSBC independently within a globla iteration loop. The following parts focus on another two key issues, i.e., coupling method and spatial mapping.

1. Coupling method

Generally, there are two methods for coupling two separate codes into one integrated system: external coupling and internal coupling. For the external coupling method, the transferring of coupling parameters is usually realized through external files. Also an extra coupling script is needed to execute the coupling calculation. This coupling approach is flexible and simple to incorporate mature codes without adapting them.

For the internal coupling method, the neutronics code and T/H code are integrated based on a same framework as two separate modules, where the coupling parameters are transferred in memory. There are two advantages of this approach. Firstly, efficiency can be enhanced by exchanging data in memory instead of external files because the latter one needs large I/O operations. Secondly, the two modules can share the geometry information, making the spatial mapping much easier. Therefore, the internal coupling method is adopted to couple NECP-X with SUBSC.

2. Spatial mapping

Currently, the following thermal-hydraulics parameters of each pin cell are used to update the cross sections for the neutronics calculation: average fuel temperature, average cladding temperature, average temperature and density of coolant surrounding the rod. Due to the difference of solution meshes, appropriate spatial mapping between NECP-X and SUBSC is important. Fig. 5 shows the spatial mapping approach for the NECP-X/SUBSC coupling. Specifically, for the coolant part, volume-weighted density and mass-weighted temperature of four channels (SUBSC index: 25, 26,35, 36) are used to update (NECP-X index: 15) the coolant cross sections for neutronics calculation.

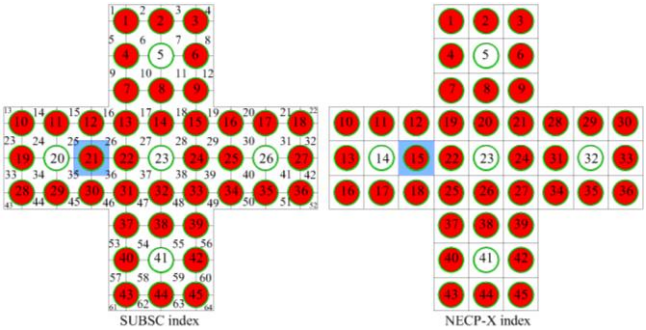

Fig. 5. Mesh mapping between NECP-X and SUBSC

For the fuel and cladding parts, benefiting from three dimensional conduction model of SUBSC, detailed 3-D distribution of temperature can be provided as illustrated in Fig. 6. However, only volume-weighted average temperatures are implemented to update fuel and cladding's cross sections in NECP-X at present. For fuel rod "i" at axial node "j", the volume-weighted fuel temperature $\overline{T}_{f(i,j)}$ can be expressed as

$$\overline{T}_{f(i,j)} = \sum_{ir=1}^{nf}\left(\frac{Af_{ir}}{Af}\right)\left(\frac{1}{nazi}\sum_{iazi=1}^{nazi} T_{ir,iazi,i,j}\right)$$

Where nf denotes the total number of radial nodes in the fuel rod; $nazi$ denotes number of azimuthal nodes; Af_{ir} denotes the cross sectional area of ir node; Af denotes the total cross sectional area of the fuel.

Similarly, the volume-weighted cladding temperature $\overline{T}_{c(i,j)}$ can be expressed as

$$\overline{T}_{c(i,j)} = \sum_{ir=1}^{nc}\left(\frac{Ac_{ir}}{Ac}\right)\left(\frac{1}{nazi}\sum_{iazi=1}^{nazi} T_{ir,iazi,i,j}\right)$$

Where Ac denotes the total cross sectional area of the cladding.

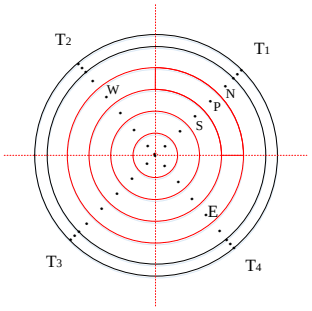

Fig. 6. 3-D temperature distribution

Linear power of each cell at each axial node is provided by NECP-X for SUBSC to update the source term of 3D conduction equation.

3. Numerical results

3.1 3x3 pin cluster case

A simplified PWR 3x3 pin cluster case is designed as shown in Fig. 7. The geometry and material are summarized in table 3.

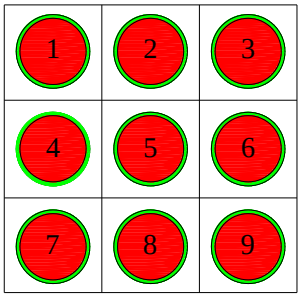

Fig. 7. 3x3 pin cluster geometry

Table 3. Geometry and material data for 3x3 pin cluster case.

Parameter	Value
Fuel outer radius	0.4096cm
Cladding inner radius	0.418cm
Cladding outer radius	0.475cm
Pitch	1.26cm
Axial height	350cm
Fuel	UO_2
Fuel enrichment	3.10%
Fuel density	10.29769g/cm^3
Cladding	Zr-4
Clad density	6.55g/cm^3
Moderator	water
Boron	0 ppm

The iteration process is shown in Table 4. It doesn't stop until a rather tight convergence criteria or the maximum iteration number is reached: 5 pcm in eigenvalue (Δk_{eff}), 1% in axial linear power (Δpower) and 0.1K in peak fuel temperature (ΔT_{fuel}). Because of the tight convergence criteria, the coupling code gets converged after 10 iterations. Both initial and converged axial normalized power distributions are given in Fig. 8. The power peak moved to the bottom part of the pin cluster compared to the initial power profile since the moderator there is denser.

Table 4. Iteration summary

Iteration	k_{eff}	Δk_{eff}/pcm	Δpower/%	ΔT_{fuel}/K
1	1.305758	-	-	-
2	1.319078	1332	102.93	157.07
3	1.314960	-411.8	50.59	63.00
4	1.316598	163.8	14.80	24.29
5	1.315918	-68	6.45	8.86
6	1.316160	24.2	2.21	3.11
7	1.316073	-8.7	0.79	1.08
8	1.316104	3.1	0.27	0.38
9	1.316093	-1.1	0.09	0.13
10	1.316097	0.4	0.03	0.05

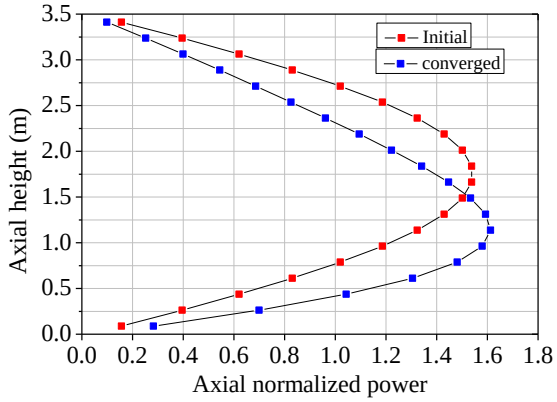

Fig. 8. Comparison of axial normalized power for initial and converged iteration

3.2 VERA 3D HFP assembly problem

The geometry of 3D HFP assembly of the VERA problem 6 is identical to that of problem 3A. The assembly power is 17.67MW. The inlet coolant temperature is 565K and bypass flow accounts for 9% of the total flow. A quarter-assembly is modelled radially due to symmetry. There are 49 axial mesh regions in the active core. Each guide tube as well as the center instrument is simulated as an unheated cylinder with water flowing inside. Heat transfer through walls of guide tube is allowed to heat the water flowing in the guide tube.

Results of eigenvalue of kinds of coupling codes are shown in Table 5. Compared to MPACT/CTF, NECP-X/SUBSC underestimates eigenvalue by 140 pcm. Relative differences of normalized radial power distribution between NECP-X/SUBSC and MPACT/CTF results are provided in Fig.9. Maximum error and RMS error are 1.30% and 0.69%, respectively. Initial and converged normalized axial power distributions of NECP-X/SUBSC are compared in Fig. 10.

Table 5. Eigenvalue for VERA 3D HFP assembly

Code	Eigenvalue
MC21/COBRA-IE	1.16431±0.00003
MPACT/CTF	1.16360
NECP-X/SUBSC	1.16220

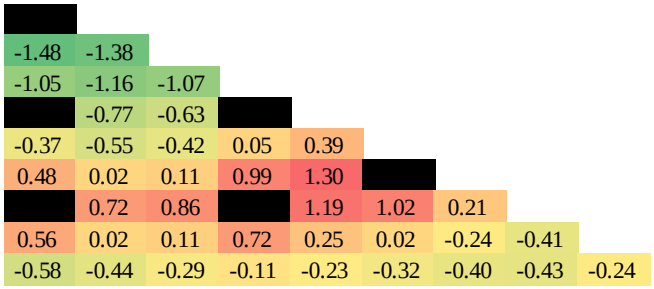

Fig. 9. Relative error of radial power distribution between NECP-X/SUBSC and MPACT/CTF

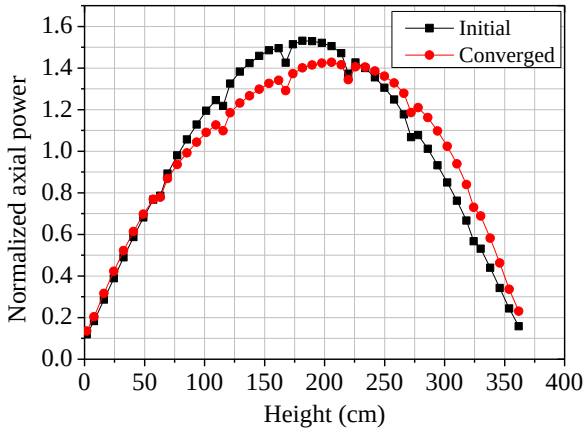

Fig. 10. Axial normalized power for initial and converged iteration

Ⅵ. CONCLUSIONS

A high-fidelity neutronics and thermal-hydrulics coupling code was developed by integrating an in-house subchannel code SUBSC with the recently developed high-fidelity neutronics code NECP-X through an internal coupling method. Improved geometry treatment such as semi-explicit representation of spacer grid, 2D/1D fusion method, as well as resonance self-shielding treatment with pesudo-resonant-nuclide subgroup method was discussed and implemented in NECP-X. Verifications were performed for VERA core physics benchmark progression problems 1-2 to investigate the accuracy. In order to avoid large negative self-scattering cross-section caused by the in-scattering based transport correction which degrades convergence of 2D/1D iteration calculation, P0 approximation for the scattering source was adopted to simulate VERA problem #3A at present. The VERA 2D and 3D benchmarks demonstrated the accuracy of NECP-X.

Thereafter, the coupling code NECP-X/SUBSC was applied to a simplified PWR 3×3 pin cluster. Various convergence metrics including eigenvalue , axial linear power and peak fuel temperature of each fuel pin were employed to tighten the convergence criteria. The coupling code converged after 10 iterations, demonstrating success of integrating SUBSC with NECP-X. Finally, VERA problem #6 was simulated. Calculated eigenvalue agreed within 140 pcm compared with result from MPACT/CTF. Normalized radial power distribution were also compared and the results showed that maximum error and RMS error were 1.30% and 0.69%, respectively. The differences may be attributed to different scattering source approximations adopted in neutronics code as well as different turbulence models, friction models and water property used in subchannel code.

ACKNOWLEDGMENTS

This work was supported by National Natural Science Foundation of China No. 11605130, 11605128 and China Postdoctoral Science Foundation No. 2015M580854,

REFERENCES

1. Turinsky P J, Kothe D B. Modeling and simulation challenges pursued by the Consortium for Advanced Simulation of Light Water Reactors (CASL)[J]. Journal of Computational Physics, 2016, 313: 367-376.
2. Short M P, Hussey D, Kendrick B K, et al. Multiphysics modeling of porous CRUD deposits in nuclear reactors[J]. Journal of nuclear materials, 2013, 443(1): 579-587.
3. Clarno K T, Pawlowski R P, Evans T M, et al. High Fidelity Model ing of Pellet-Clad Interaction Using the

CASL Virtual Environment for Reactor Applications[C]//Proceedings of the ANS Joint International Conference on Mathematics and Computation (M&C 2015), Supercomputing in Nuclear Applications (SNA) and the Monte Carlo (MC) Method, Nashville, TN, USA. 2015.
4. Jung Y S, Shim C B, Lim C H, et al. Practical numerical reactor employing direct whole core neutron transport and subchannel thermal/hydraulic solvers[J]. Annals of Nuclear Energy, 2013, 62: 357-374.
5. Kochunas B, Jabaay D, Collins B, et al. Demonstration of Neutronics Coupled to Thermal-Hydraulics for a Full-Core Problem using COBRA-TF/MPACT[J]. CASL Document, CASL-U-2014-0051-000, 2014.
6. Aviles B, Kelly D, Aumiller D, et al. Coupled MC21 and COBRA-IE Solution to VERA Core Physics Benchmark Problem# 6 [C]//Proc. Int. Conf. Unifying Theory and Experiments in the 21st Century (PHYSOR 2016), Sun Valley, Idaho, USA, May. 2016: 1-5.
7. Daeubler M, Ivanov A, Sjenitzer B L, et al. High-fidelity coupled Monte Carlo neutron transport and thermal-hydraulic simulations using Serpent 2/SUBCHANFLOW[J]. Annals of Nuclear Energy, 2015, 83: 352-375.
8. L.Liang, Z.Y.Liu, H.C.Wu et al, "Leakage reconstruction method for 2D/1D fusion transport calculations". Progress in Nuclear Energy 97(2017) 60-73.
9. C Zhao, et al. The iteration and parallel strategy for the 2D/1D transport method in NECP-X [C]//International Conference on Mathematics & Computational Methods Apploed to Nuclear Science & Engineering, April 16-20, Jeju, Korea. 2017.
10. Li Y, He Q, Cao L, et al. Resonance elastic scattering and interference effects treatments in subgroup method[J]. Nuclear Engineering and Technology, 2016, 48(2): 339-350.
11. He Q, Cao L, Wu H, et al. Improved resonance calculation of fluoride salt-cooled high-temperature reactor based on subgroup method[J]. Annals of Nuclear Energy, 2016, 88: 204-217.
12. Schmidt R, Belcourt N, Hooper R, et al. An Introduction to LIME 1.0 and its Use in Coupling Codes for Multiphysics Simulations[J]. Sandia National Laboratories, Albuquerque, NM, 2011.
13. Godfrey A T. VERA core physics benchmark progression problem specifications[J]. Oak Ridge National Laboratory, CASL-U-2012-0131-004, 2013.